Analyst

RSC Publishing

PAPER

View Article Online
View Journal | View Issue

Cite this: *Analyst*, 2013, **138**, 4475

A novel microfluidic mixer based on dual-hydrodynamic focusing for interrogating the kinetics of DNA–protein interaction†

Ying Li,‡ Fei Xu,‡ Chao Liu, Youzhi Xu, Xiaojun Feng and Bi-Feng Liu*

Kinetic measurement of biomacromolecular interaction plays a significant role in revealing the underlying mechanisms of cellular activities. Due to the small diffusion coefficient of biomacromolecules, it is difficult to resolve the rapid kinetic process with traditional analytical methods such as stopped-flow or laminar mixers. Here, we demonstrated a unique continuous-flow laminar mixer based on microfluidic dual-hydrodynamic focusing to characterize the kinetics of DNA–protein interactions. The time window of this mixer for kinetics observation could cover from sub-milliseconds to seconds, which made it possible to capture the folding process with a wide dynamic range. Moreover, the sample consumption was remarkably reduced to <0.55 μL min^{-1}, over 1000-fold saving in comparison to those reported previously. We further interrogated the interaction kinetics of G-quadruplex and the single-stranded DNA binding protein, indicating that this novel micromixer would be a useful approach for analyzing the interaction kinetics of biomacromolecules.

Received 15th March 2013
Accepted 21st May 2013

DOI: 10.1039/c3an00521f

www.rsc.org/analyst

Introduction

Kinetics investigation of chemical or biochemical reaction is of great importance since it provides insight into the reaction mechanism.[1–4] Biochemical reactions among biomacromolecules within living cells such as DNA hybridization,[5] DNA–protein binding[6,7] and protein–protein interaction[8] play important roles in many cellular activities including the regulation of gene expression, replication, and repair of DNA damage.[9,10] Investigating the kinetics of these processes is essential for understanding the molecular basis for cellular functions.[11–14]

The stopped-flow method is the conventional approach for kinetic measurements.[15,16] Coupled with optical detections such as fluorescence imaging[17] and circular dichroism,[18] stopped-flow methods have provided valuable information on the mechanisms of nuclei acid and protein folding. However, the millisecond dead time and large sample consumption (about 1 mL per test) restrict its widespread applications.[2,19] In recent years, the concept of continuous-flow has been widely accepted in the microfluidic mixer to analyze the kinetics of chemical and biological reactions due to its rapid mixing time.[20–23] Current continuous-flow micromixers could be generally categorized into turbulent mixers and laminar mixers. In turbulent mixers, fluids are pressurized to flow through irregular channels with high velocity. Thus, complete mixing could be realized by chaotic advection in tens of microseconds.[24–28] Turbulent mixers could mix solutions with various molecular weights. However, the reagent consumption was still relatively high (10 mL min^{-1},[25] 1.2 mL min^{-1},[26,27] and 0.6 mL min^{-1}),[28] leading to high cost of purified protein and DNA samples in the experiments. As an alternative to the turbulent micromixer, the laminar mixer could achieve complete mixing in the microsecond time scale through hydrodynamic focusing.[20,22,23] In this method, the fluid containing macromolecules was sandwiched into a thin line by two side streams of low-mass-molecule solutions.[19,21] Small molecules from the side channel diffused rapidly through the thin layer and triggered the kinetic reaction. Therefore, the consumption of the macromolecule was minimized to several nanoliters per second at the cost of high consumption of inexpensive small molecules.[22,29] However, these laminar mixers were restricted to the investigation of the interaction kinetics between biomacromolecules and small molecules, *e.g.*, the protein folding kinetics initiated by diluting high concentrations of GuHCl[23] or binding of SDS.[21] It seemed that previous laminar mixers were inapplicable to characterize the interaction kinetics between two kinds of biomacromolecules, owing to the slow diffusion of macromolecules and high consumption of expensive samples in the side channels. Thus, it is difficult for previous microfluidic mixers to

Britton Chance Center for Biomedical Photonics at Wuhan National Laboratory for Optoelectronics-Hubei Bioinformatics & Molecular Imaging Key Laboratory, Systems Biology Theme, Department of Biomedical Engineering, College of Life Science and Technology, Huazhong University of Science and Technology, Wuhan 430074, China. E-mail: bfliu@mail.hust.edu.cn; Fax: +86-27-8779-2170; Tel: +86-27-8779-2203

† Electronic supplementary information (ESI) available. See DOI: 10.1039/c3an00521f

‡ These authors contributed equally to this work.

resolve the interaction kinetics between biomacromolecules with short mixing time and low sample consumption.

In this work, we proposed a new laminar micromixer based on microfluidic dual-hydrodynamic focusing to interrogate biomacromolecular interaction kinetics. The dual-hydrodynamic focusing was achieved by simultaneously focusing the two central sample solutions through sheath flow. Mixing efficiency was characterized by both numerical simulations and experiments with fluorescent molecules of low and high molecular weights. Under optimized conditions, the mixer could achieve a sub-millisecond mixing time and the observation time window covered four orders of magnitude (710 μs to 5.36 s). Consumption of the two kinds of macromolecules was less than 0.55 μL min^{-1}, over 1000-fold saving in comparison to previous reports. Bioluminescent reaction validated the reliability of this micromixer for analyzing the kinetics of biochemical reactions. Emphasis was further placed on tracking the interaction kinetics between the human telomere G-quadruplex and the single-stranded DNA binding protein (SSBP). This micromixer offers unique advantages of low sample consumption and wide dynamic time range, making it an ideal tool for characterizing the interaction kinetics of macromolecules.

Experimental

Computational fluid dynamics (CFD) simulations

Numerical simulation was carried out to quantify the mixing performance of the micromixer by COMSOL multiphysics™ (COMSOL 3.4, Sweden). The flow profile was investigated using a 2D finite element model. The simulation was performed by solving the incompressible Navier–Stokes equations and the convective-diffusion equation.[22,30]

$$\rho\frac{\partial u}{\partial \tau} + \rho u\cdot\nabla u = -\nabla P + \mu\nabla^2 u \quad (1)$$

$$\nabla\cdot u = 0 \quad (2)$$

$$\frac{\partial u}{\partial \tau} + Du\cdot\nabla c = D\nabla^2 c \quad (3)$$

where ρ, τ, u, P, μ, c and D are the density, the time, the velocity vector, the pressure, the dynamic viscosity, the concentration of the species and the molecular diffusion, respectively. Newtonian fluid was used in the simulation with a density (ρ) of 10^3 kg m^{-3} and a viscosity (μ) of 10^{-3} Pa s. A diffusion coefficient (D) of 1×10^{-9} m^2 s^{-1} was used for small molecules of low weight and 1×10^{-10} m^2 s^{-1} for large molecules of high weight.

Chip fabrication

Microfluidic devices were fabricated using a rapid prototyping method as reported previously.[31] The PDMS (Sylgard 184, Dow Corning, USA) layer with the microchannel was obtained by prototyping against SU-8 (2100, Gersteltec Sarl, Switzerland) masters. Access holes were punched at the ends of PDMS channels with a syringe needle. The PDMS was irreversibly bonded to a glass slide after oxygen plasma treatment. Steel needles attached with teflon tubes were inserted into the punched holes and fixed with epoxy glue to form the final device. The height of the microchannels was 25 μm. A schematic of the microchannel design is shown in Fig. 1a and the final device is shown in Fig. 1b.

Materials and sample preparation

Chemicals such as $Na_2B_4O_7\cdot 10H_2O$, HCl, NaOH, NaC, K_2HPO_4, KH_2PO_4, H_2O_2, EGTA, Tris, and fluorescein ($M_w = 332.31$) were purchased from Sinopharm Chemical Reagent (Shanghai, China). Fluorescein-labeled dextran ($M_w = 500\,000$) and tetramethylrhodamine-labeled dextran ($M_w = 70\,000$) were obtained from Molecular Probes (Eugene, OR, USA). Horseradish peroxidase (HRP) was purchased from Beijing biosynthesis biotechnology Co., Ltd (Beijing, China). Luminol was purchased from Wako (Japan) and 4-iodophenol was purchased from Alfa Aeser (USA). The single-stranded DNA binding protein (SSBP) was purchased from Promega (USA). Bovine serum albumin (BSA) was purchased from Solarbio (Beijing, China). The oligonucleotide ($d(TTAGGG)_4$) was purchased from TaKaRa Biotech (Dalian, China). The oligonucleotide ($d(TTAGGG)_4$) was labeled with 5′-fluorescein (FAM) and 3′-tetramethylrhodamine (TMR) and purified by HPLC.

Solutions of 1.0 μM fluorescein, fluorescein–dextran and tetramethylrhodamine–dextran were dissolved in 0.1 M borate buffer (pH 11.0). The bioluminescence (BL) reagent (containing 2.5 mM luminol, 100 mM H_2O_2 and 4.5 mM 4-iodophenol) was dissolved in 0.1 M phosphate buffer (pH 11.0). Stock solution of 5×10^{-5} M HRP was dissolved in 0.01 M phosphate buffer (pH 6.8). Lower concentrations of HRP were diluted from the stock solution before use.

The 1 μM oligonucleotide ($d(TTAGGG)_4$) was dissolved in Tris–HCl buffer (10 mM Tris, pH 7.4, 1.0 mM EDTA), in which various concentrations of NaCl were added. SSBP and BSA were dissolved in the Tris–HCl buffer with a final concentration of 0.5 μM. The oligonucleotide samples were incubated at 95 °C for 5 min and then slowly cooled down to room temperature before the analysis.

All solutions were prepared with water purified by the Direct-Q system (Millipore, Bedford, MA, USA) and filtered with 0.45 μm sterilized syringe filters prior to use.

Optical imaging system

Experiments were performed on an inverted fluorescence microscope (IX71, Olympus, Japan) with a CCD camera (Evolve 512, photometrics, USA). Objectives of 10× (NA 0.3) and 20× (NA 0.45) were used. Mixing of fluorescein solution and borate buffer was examined with a filter cube of U-MWIB2 (460–490 nm band-pass filter, 505 nm dichroic mirror, 510 nm high-pass filter, Olympus, Japan). Mixing of fluorescein–dextran and tetramethylrhodamine–dextran was examined with filter cubes of U-MWIB2 and U-MWG2 (510–550 nm band-pass filter, 570 nm dichroic mirror, 590 nm high-pass filter, Olympus, Japan). The luminescence of BL reaction was collected with a 420 nm high-pass emission filter.

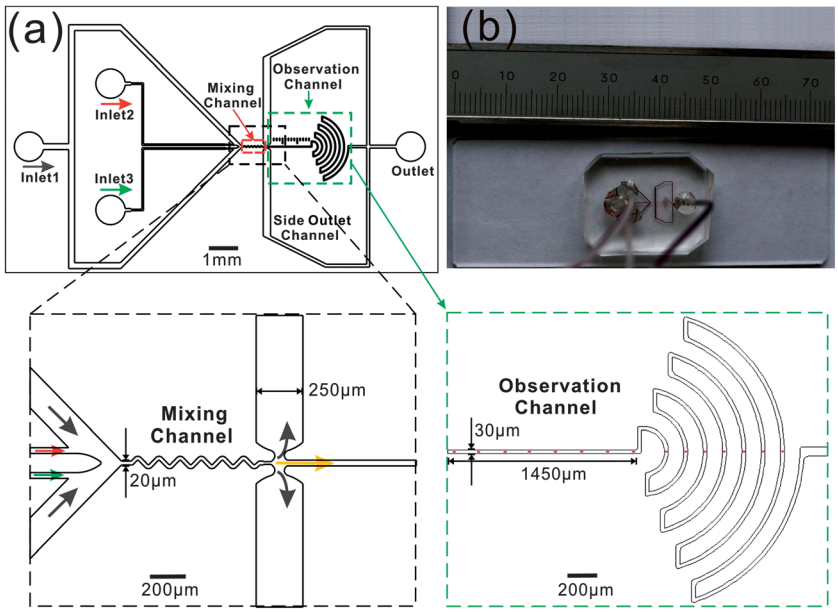

Fig. 1 (a) Schematic of the microchannel of the micromixer. The bottom insets were the enlarged view of the black and green rectangle boxes in (a). The red dot in the right inset showed the region of interest (ROI). (b) The fabricated micomixer (ruler unit: mm).

A laser scanning confocal microscope (LSCM, FV1000, Olympus, Japan) was used as the platform for monitoring the mixing of fluorescent molecules and the interaction kinetics between the G-quadruplex and SSBP. An argon laser (λ = 488 nm) and a He–Ne laser (λ = 543 nm) were used as the light source. The objectives used were 10× (NA 0.3) and 20× (NA 0.45). The exposure time of each pixel was 20 μs. The oligonucleotide with 5′-FAM and 3′-TMR was excited with 488 nm and the emission fluorescence was collected at 510–550 nm for FAM and 565–605 nm for TMR.

Operation procedures

Fluid was transported in the device by compressed air in a continuous manner. As shown in Fig. S1,† the pressures could be finely tuned to achieve the desired flow rates.

The hydrodynamic focusing profile was evaluated using fluorescein and borate buffer. Fluorescein was loaded into inlet 2, while borate buffer was loaded into inlet 1 and inlet 3. Further evaluation of the mixing efficiency was conducted with fluorescein–dextran and tetramethylrhodamine–dextran injected into the two central channels and the borate buffer injected into the side channel.

To characterize the kinetics of BL reaction, the phosphate buffer was injected into the side channel from inlet 1, while the BL reagent and various concentrations of HRP were injected into the two central channels from inlet 2 and inlet 3, respectively.

Investigation of the interaction kinetics was monitored by fluorescence resonant energy transfer (FRET) through the mixing of 1 μM DNA (d(TTAGGG)$_4$) solution (containing various concentrations of NaCl) and 0.5 μM SSBP. Tris–HCl buffer was injected into the side channel from inlet 1, while DNA solution and SSBP were injected into inlet 2 and inlet 3. 5′-FAM served as the donor and 3′-TMR as the acceptor. Acquired images were analyzed using Image Pro Plus 6.0, Matlab 7.0 and Origin 7.5.

Results and discussion

Strategy of microfluidic dual-hydrodynamic focusing

Hydrodynamic focusing has been widely used in laminar micromixers pioneered by Brody *et al.*[20] The sample in the central channel was focused into a narrow stream and rapid mixing was achieved through the diffusion of the small molecules in the side channels. However, it could not meet the requirement for investigating the interaction kinetics between biomacromolecules. To overcome this problem, we demonstrated a new strategy of dual-hydrodynamic focusing in the microfluidic mixer. As shown in Fig. 1a, buffer solution was injected into inlet 1, while the two samples of biomacromolecules were introduced from inlet 2 and inlet 3. With appropriate adjustment of the flow rates, both the samples were focused into a thin stream with the help of the sheath flow, which minimized the consumption of expensive samples. The focused samples achieved rapid mixing in the downstream serpentine mixing channel and the interaction kinetics was monitored in the observation channel. In consideration of the interaction between biomacromolecules occurring very fast in a wide dynamic time range,[32,33] we designed a four-way junction (downstream of the mixing channel) similar to the configuration proposed by Gambin *et al.*,[21] which diverted the buffer solution and the sample solution into the side outlet and the observation channel respectively. Thus, the flow velocity in the observation channel was decreased about three orders compared to that in the mixing channel and it resulted in a long observation time window.

CFD simulation

Numerical simulations were carried out to characterize the flow pattern of the dual-hydrodynamic focusing mixer (Fig. 2). As shown in Fig. 2a, sample solution of 1.0 M (molecular diffusion coefficient, 1×10^{-9} m^2 s^{-1}) was loaded into inlet 1, while buffer was loaded into inlet 2 and inlet 3. The pressure at the two central inlets (Pc) was set to 35 kPa, while the pressure at inlet 1 (Ps) was increased from 1 to 35 kPa. At the four-way junction, the fluid was divided into three sub-flows, which flowed into the observation channel and the two side channels, respectively. With the increase of Ps/Pc, the width of the focused central stream (w_c) became smaller and more amount of the central stream was diverted into the observation channel (Video S1†). When Ps was increased to 35 kPa, most of the focused central stream flowed into the observation channel, with minimal loss into the two side output channels.

To evaluate the mixing efficiency of two kinds of macromolecules in the mixer, inlet 1 was fed with a solution of 0.5 M, while inlets 2 and 3 were fed with a solution of 1.0 M (molecular diffusion coefficient, 1×10^{-10} m^2 s^{-1}) and 0 M, respectively. As the Ps/Pc ratio increased, w_c became narrower and the diffusion distance between the samples decreased (Fig. 2b and Video S2†). The solutions achieved a better mixing efficiency (C_m) at larger Ps/Pc, and the colour images demonstrated that the two samples realized complete mixing ($C_m = 0.95$) at the entrance of the observation channel when the Ps/Pc ratio was 35 : 35 (the right inset in Fig. 2b). Here C_m was calculated according to the following equation:[27,34]

$$C_m = 1 - \frac{\sqrt{\sum (X_i - \overline{X})^2 / N}}{\overline{X}},$$

where X_i is the intensity of each point in the cross-section, N is the number of total points and $\bar{X}$ is the average intensity of all the points. The value of C_m ranged between minimum 0% and maximum 100% and larger C_m indicated better mixing efficiency. According to the previous report,[22,27] a C_m of above 0.9 was recognized as a complete mixing.

To test whether the pressures would influence the mixing efficiency, we changed the pressure Pc (set as 5 kPa, 10 kPa, 25 kPa, 45 kPa, 65 kPa, 75 kPa, and 85 kPa) while kept the ratio of Ps/Pc. Results demonstrated that the flow profile was almost the same as that of Pc = 35 kPa at the same ratio of Ps/Pc (data not shown).

Experimental evaluation of the micromixer

To check the performance of the dual-hydrodynamic focusing mixer, solutions of low molecule weights (fluorescein and borate buffer) were used at first. The experiments were conducted with fluorescein injected into inlet 2 while buffer injected into inlet 1 and inlet 3. The flow profile in Fig. 3a showed that more amount of the central sample was diverted into the observation channel under larger Ps/Pc (Pc was set as 35 kPa). The different lines in Fig. 3b indicated that fluorescence in the observation channel distributed more and more homogeneously with increasing Ps/Pc. Fig. 3c further demonstrated that the two small molecules reached complete mixing after flowing through the serpentine channel when Ps and Pc were both 35 kPa. (In the case of a straight channel, the mixing efficiency was poor as shown in Fig. S2.†) Similar to the simulation, we found that the width of the focused stream and mixing efficiency did not depend on the magnitude of the applied pressures, but rather on the ratio of Ps/Pc. The ESI (Video S3 and S4†) shows the results at various ratios of Ps/Pc when Pc was 35 and 75 kPa.

To further test the mixing efficiency of the mixer for macromolecules, two fluorescent tagged molecules (fluorescein–dextran

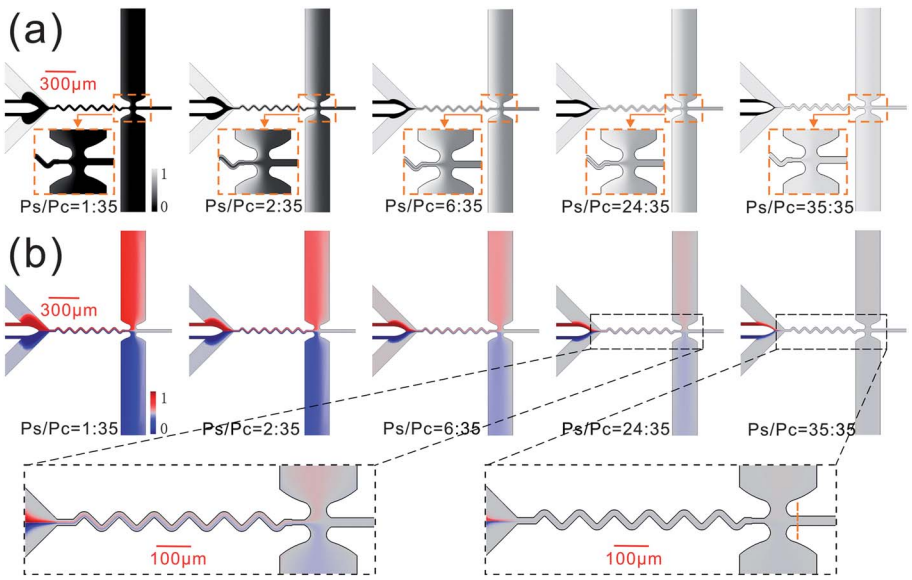

Fig. 2 Simulation results of the micromixer under various Ps/Pc when Pc was 35 kPa (Ps, the pressure used at inlet 1; Pc, the pressure used at inlet 2 and inlet 3; pressure unit: kPa). (a) The result of group 1 (the solution concentration was set as 1.0 M, 0 M, 0 M for inlet 1, inlet 2 and inlet 3, respectively). The insets were the enlarged views of the area indicated by the orange dotted rectangle boxes. (b) The result of group 2 (the solution concentration at inlet 1, inlet 2 and inlet 3 was 0.5 M, 1.0 M and 0 M, respectively). The bottom insets were the enlarged views of the area indicated by the black dotted rectangle boxes.

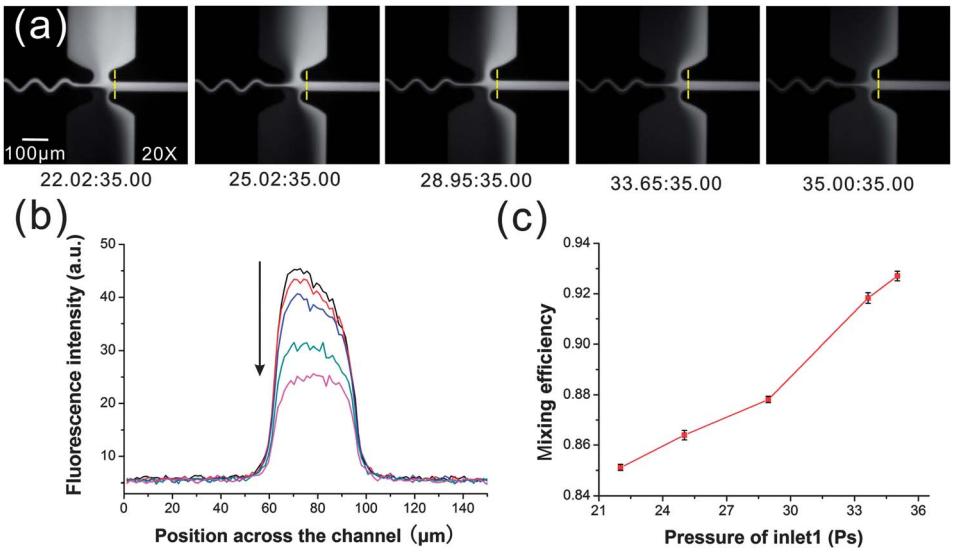

Fig. 3 Mixing results of fluorescein and borate buffer with low molecular weights (Ps, the pressure used at inlet 1; Pc, the pressure used at inlet 2 and inlet 3; pressure unit: kPa). (a) The flow pattern under various Ps/Pc (Pc was set as constant, 35 kPa). Inlet 1 and inlet 3 were feeding with buffer, while inlet 2 was feeding with fluorescein. The objective used was 20× (NA 0.45). (b) The fluorescence distribution at the position of the yellow dotted lines shown in (a). The curves from the top to bottom represented the results from low Ps/Pc to high Ps/Pc. (c) The mixing efficiency at various ratios of Ps/Pc at the position of the yellow dotted lines shown in (a).

and tetramethylrhodamine–dextran) of high molecular weight (500 000 Da and 70 000 Da) were used. The result under various Ps/Pc (Pc = 35 kPa) was monitored with a 10× objective as shown in Fig. 4a. When Ps increased to 35 kPa, the fluorescence in the observation channel became homogenous. The resulting images (*X*–*Y* plane) at Ps/Pc = 35 : 35 were obtained using a 20× objective and are shown in Fig. 4b with pseudo-colour. The insets (*Y*–*Z* plane) were the reconstructed cross-sections given by LSCM, which demonstrated homogeneous fluorescence distribution for each slice along the *Z*-axis. The fluorescence distribution shown in Fig. 4c further demonstrated that the two fluorescent molecules achieved complete mixing (C_m was 0.92 for fluorescein–dextran and 0.93 for tetramethylrhodamine–dextran).

Mixing dead time and observation time window

The sample solutions from the two central inlet channels realized complete mixing after flowing through the serpentine mixing channel at Ps/Pc = 1. To calculate the mixing dead time of the micromixer, the pressure ratio of Ps/Pc was kept 1 : 1, while Pc was increased from 12 kPa to 85 kPa. According to the flow rate in the observation channel (data from the section of 'flow rate calibration' in the ESI†) and the channel size (the total

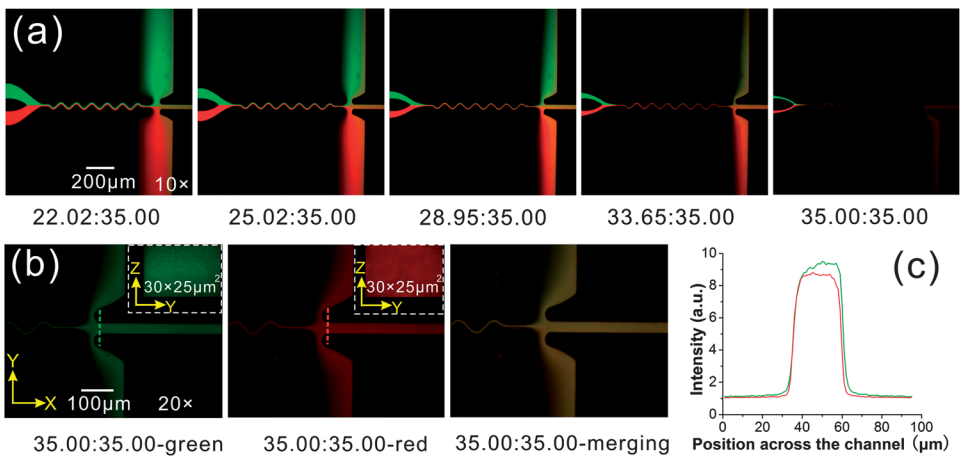

Fig. 4 Mixing results of the two solutions (fluorescein–dextran, M_w = 500 000 and tetramethylrhodamine–dextran, M_w = 70 000) of high molecular weights. (a) Flow patterns under various Ps/Pc (Ps was set as 35 kPa, pressure unit: kPa). Inlet 1 was fed with buffer, while inlet 2 and inlet 3 were fed with fluorescein–dextran and tetramethylrhodamine–dextran, respectively. The objective used was 10× (NA 0.3). (b) Mixing result of the two fluorescent molecules at Ps/Pc = 35 : 35 monitored with an objective of 20× (NA 0.45). The insets (30 × 25 μm²) were the reconstructed cross-sections given by LSCM at the position of the green and red dotted line. (c) The fluorescence distribution of fluorescein–dextran (green) and tetramethylrhodamine–dextran (red) at the position of the green and red dotted line shown in (b).

Table 1 Mixing time and observation time window responding to the pressure (Pc)

Pressure (kPa)	Mixing time (ms)	Observation time window (s)	Pressure (kPa)	Mixing time (ms)	Observation time window (s)
12	5.88	44.12	55	1	7.5
25	2.48	18.6	65	0.9	6.72
35	1.64	12.3	75	0.71	5.36
45	1.32	9.91	85	0.66	4.91

length of the mixing channel was 1.0 mm and the channel height was 25 μm), we converted the Eulerian space coordinate to the Lagrangian time coordinate.[19,22] The relationship between the pressure Pc and the mixing dead time or the observation time window is shown in Table 1. The time zero for mixing was set at the entrance of the mixing channel, while the time zero for observation was set at the entrance of the observation channel. Since low pressures resulted in small flow rates, the mixing dead time and the observation time window were long at low pressures. When Pc was 35 kPa, the mixing dead time was 1.64 ms and the observation time window was 12.3 s. If Pc was increased to 75 kPa, the mixing dead time was decreased to 710 μs and the observation time window would be 5.36 s, which demonstrated that the observation time window could cover four orders of magnitude in the time range.

Kinetic analysis of bioluminescence reaction

Bioluminescence (BL) detection has advantages of wide linear range, no requirement for light source and reduced analysis time.[35] Luminol BL reaction catalyzed by HRP is usually coupled with immunoassay to quantitatively analyze antibody and antigen.[36,37] To investigate the kinetics of the BL reaction, the BL reagent and various concentrations of HRP were injected into inlet 2 and inlet 3 while buffer was injected into inlet 1. The pressure used for the three inlets was set as 75 kPa and the flow rate of the two samples was 0.52 μL min^{-1} (Fig. S3b†). In Fig. 5, the kinetic process of the BL reaction at different HRP concentrations was demonstrated. Since the BL reaction was triggered immediately when the reagents met (Video S5†), data of the mixing channel and the observation channel were both extracted. The average velocity was 1.4 m s^{-1} in the mixing channel, while it was only 2.3 mm s^{-1} in the observation channel. As shown in Fig. 5, the data before the *X*-axis break were extracted from the mixing channel and demonstrated a rapid rise phase and a fall phase in a very short time. The data after the *X*-axis break were extracted from the observation channel, which revealed a slow decrease phase of luminescence intensity. The ESI (Video S5†) shows the reaction process in the whole channel. This experiment revealed that the dual-hydrodynamic focusing mixer was a reliable tool for analyzing the kinetics of chemical or biochemical reactions.

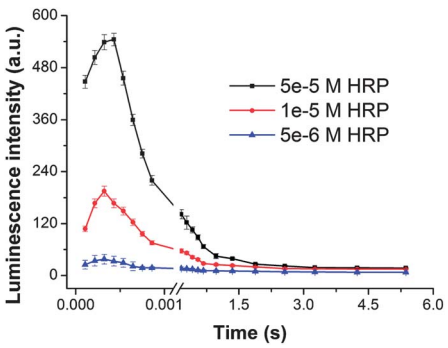

Fig. 5 The kinetic process of luminol–HRP BL reaction. To demonstrate the whole kinetic process of the reaction, the zero point was set at the entrance of the mixing channel. The data before and after the break of the *X*-coordinate were extracted from the mixing channel and the observation channel, respectively.

Interaction kinetics of G-quadruplex and SSBP

The G-rich strand of the human telomere DNA sequence $(d(TTAGGG)_4)$, an essential structure to aging and cancer therapy,[38,39] can form four stranded structures called G-quadruplexes. Quadruplexes arise due to the ability of guanine to hydrogen bond in a cyclic fashion,[40] which are further stabilized by the coordination of interstitial cations (*e.g.*, Na^+ and K^+).[41] SSBP is essential for DNA function in prokaryotic and eukaryotic cells, mitochondria, phages and viruses.[10] SSBP was reported to bind single-stranded DNA with high specificity but not bind to double-stranded DNA.[42] As SSBP has the ability to distinguish the unfolded and the folded form of DNA by DNA-binding, it was utilized to detect DNA quadruplex.[43] Here, with the new micromixer, we characterized the interaction kinetics between SSBP and the G-quadruplex, a process of how SSBP opened the folded structure of G-quadruplex.

The oligonucleotides $(d(TTAGGG)_4)$ were labeled with 5′-fluorescein (FAM) and 3′-tetramethylrhodamine (TMR). Various concentrations of NaCl (0, 50 mM, 100 mM, 150 mM) were added into the DNA solution, making the linear oligonucleotides to form folded G-quadruplexes. The Tris–HCl buffer was injected into inlet 1, while inlet 2 and inlet 3 were fed with SSBP and G-quadruplex solution respectively. The pressure used for the three inlets was 35 kPa and the flow rate of the central two samples was 0.27 μL min^{-1} (Fig. S3b†). Fluorescence images of the donor and acceptor were snapped simultaneously using the LSCM. The FRET efficiency was expressed as proximity ratio I using the definition:[44]

$$I = \frac{I_a}{I_a + I_d},$$

where I_a and I_d were the fluorescence intensities of the acceptor (TMR) and the donor (FAM), respectively. To track the unfolding process of the G-quadruplex with SSBP, the fluorescence data of the region of interest (ROI, as shown in the bottom inset of Fig. 1) were extracted and averaged to calculate the FRET efficiency. The FRET efficiency was plotted *versus* the Lagrangian time coordinate, which is shown in Fig. 6a (the entrance of the observation channel was set as time zero). Since the oligonucleotides were linear in the Tris–HCl buffer (Control 1, 0 mM Na^+), there was no G-quadruplex formed. Thus no interaction occurred between G-quadruplex and SSBP. The kinetic curve

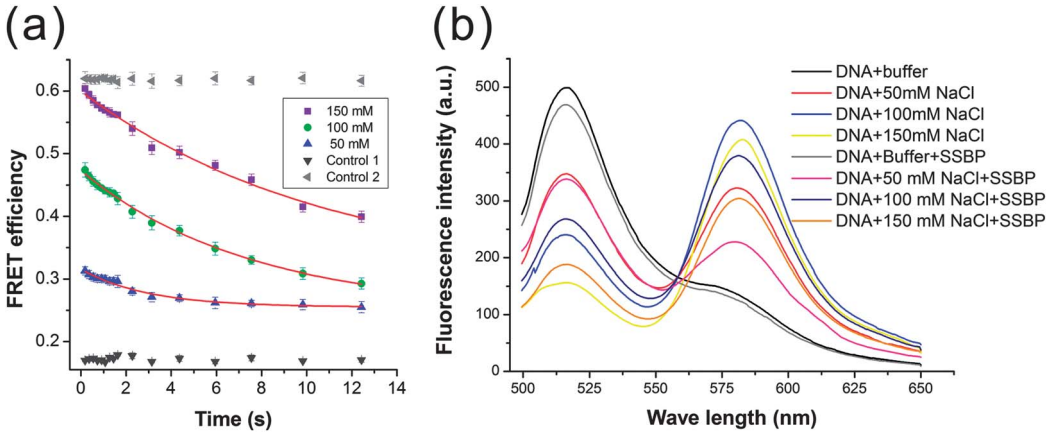

Fig. 6 (a) The interaction kinetics between the human telomere G-quadruplex and single-stranded DNA binding protein (SSBP). In Control 1, the mixing solutes were linear oligonucleotides (0 mM NaCl) and SSBP. In Control 2, the mixing solutes were G-quadruplex (150 mM NaCl) and bovine serum albumin (BSA). The data were extracted from the observation channel (ROI), shown as the red dot in the bottom inset of Fig. 1. The entrance of the observation channel was set as time zero. (b) Fluorescence spectroscopy of the G-quadruplex under different conditions.

showed a baseline. In the presence of Na^+, the formation of a compact structure of G-quadruplex led to a high FRET efficiency, and the initial FRET efficiency of the G-quadruplex was quite dependent on the concentration of Na^+, which fit well with the fluorescence spectroscopy (Fig. 6b). After the binding of SSBP, the FRET efficiency decreased as the opening of G-quadruplex[43] (fit well with Fig. 6b and Table S1†). To exclude potential contributions from non-specific interactions, a parallel experiment was done as Control 2, in which BSA was mixed with G-quadruplex (150 mM Na^+) solution. The FRET efficiency was relatively high but the value remained nearly the same in the observation channel. A similar FRET efficiency curve was also observed for mixing G-quadruplex (150 mM Na^+) with Tris–HCl buffer (data not shown). It revealed that no interaction occurred between G-quadruplex and BSA, which was confirmed by the fluorescence spectroscopy in Fig. S4.† Thus, these results validated that the unfolding of G-quadruplex was induced by the binding of SSBP. The decay curves of the experimental group (50 mM, 100 mM, 150 mM Na^+) in Fig. 6a could be fitted by a single exponential function as expected for the pseudo first-order kinetics and the observed kinetics were $0.232 \pm 0.008\ s^{-1}$, $0.097 \pm 0.005\ s^{-1}$, $0.063 \pm 0.002\ s^{-1}$, respectively. This result demonstrated that the unfolding rate of G-quadruplex with the help of SSBP decreased as the concentration of Na^+ increased. It meant that a more stable structure of quadruplex at higher concentration of Na^+ was formed, which was consistent with the previous reports.[45,46]

Conclusion

In this paper, we reported a novel continuous-flow laminar micromixer based on dual-hydrodynamic focusing. The mixing efficiency was evaluated using numerical simulations and experiments. The mixer could realize complete mixing of two kinds of macromolecules in sub-milliseconds and consumption of the two samples was reduced about 1000-fold in comparison to previous reports. Moreover, the observation time window of this mixer could cover four orders of magnitude from 710 μs to 5.35 s under the optimized conditions. The kinetic process of the BL reaction was monitored with this mixer. Furthermore, the interaction kinetics between G-quadruplex and SSBP was investigated. The results revealed that the unfolding process of G-quadruplex with the help of SSBP could be fitted well with a single exponential function. With advantages of ultra-low sample consumption and four orders of magnitude in observation time window, the proposed dual-hydrodynamic focusing micromixer could be potentially useful in characterizing the interaction kinetics of macromolecules, such as DNA hybridization, DNA–protein binding, protein–protein interaction, immuno-recognition, *etc.*

Acknowledgements

The authors gratefully acknowledge the financial supports from National Basic Research Program of China (2011CB910403), National Natural Science Foundation of China (30970692, 21075045 and 21275060).

Notes and references

1 Y. Xue, J. Q. Liu, K. W. Zheng, Z. Y. Kan, Y. H. Hao and Z. Tan, *Angew. Chem., Int. Ed.*, 2011, **50**, 8046–8050.
2 Y. Gambin, C. Simonnet, V. VanDelinder, A. Deniz and A. Groisman, *Lab Chip*, 2010, **10**, 598–609.
3 Y. Xu, X. Feng, W. Du, X. Liu, Q. Luo and B. F. Liu, *Anal. Chem.*, 2008, **80**, 6935–6941.
4 Y. Zhao, Z. Y. Kan, Z. X. Zeng, Y. H. Hao, H. Chen and Z. Tan, *J. Am. Chem. Soc.*, 2004, **126**, 13255–13264.
5 A. Murakami, M. Nakaura, Y. Nakatsuji, S. Nagahara, Q. Tran-Cong and K. Makino, *Nucleic Acids Res.*, 1991, **19**, 4097–4102.
6 M. Kanoatov and S. N. Krylov, *Anal. Chem.*, 2011, **83**, 8041–8045.
7 Q. H. Wan and X. C. Le, *Anal. Chem.*, 2000, **72**, 5583–5589.

8 D. Gerber, S. J. Maerkl and S. R. Quake, *Nat. Methods*, 2009, **6**, 71–74.
9 A. Sancar, L. A. Lindsey-Boltz, K. Unsal-Kacmaz and S. Linn, *Annu. Rev. Biochem.*, 2004, **73**, 39–85.
10 C. Wolberger, *Annu. Rev. Biophys. Biomol. Struct.*, 1999, **28**, 29–56.
11 J. W. Choi, D. K. Kang, H. Park, A. J. deMello and S. I. Chang, *Anal. Chem.*, 2012, **84**, 3849–3854.
12 D. Zhang, M. Lu and H. Wang, *J. Am. Chem. Soc.*, 2011, **133**, 9188–9191.
13 X. Niu, F. Gielen, J. B. Edel and A. J. deMello, *Nat. Chem.*, 2011, **3**, 437–442.
14 M. Srisa-Art, E. C. Dyson, A. J. deMello and J. B. Edel, *Anal. Chem.*, 2008, **80**, 7063–7067.
15 R. Russell, I. S. Millett, M. W. Tate, L. W. Kwok, B. Nakatani, S. M. Gruner, S. G. Mochrie, V. Pande, S. Doniach, D. Herschlag and L. Pollack, *Proc. Natl. Acad. Sci. U. S. A.*, 2002, **99**, 4266–4271.
16 T. Kiefhaber, *Proc. Natl. Acad. Sci. U. S. A.*, 1995, **92**, 9029–9033.
17 S. Christensen, L. Sottrup-Jensen and U. Christensen, *Biochem. J.*, 1995, **305**, 97–102.
18 B. Borucki, H. Otto, G. Rottwinkel, J. Hughes, M. P. Heyn and T. Lamparter, *Biochemistry*, 2003, **42**, 13684–13697.
19 H. Roder, K. Maki and H. Cheng, *Chem. Rev.*, 2006, **106**, 1836–1861.
20 J. P. Brody, P. Yager, R. E. Goldstein and R. H. Austin, *Biophys. J.*, 1996, **71**, 3430–3441.
21 Y. Gambin, V. VanDelinder, A. C. Ferreon, E. A. Lemke, A. Groisman and A. A. Deniz, *Nat. Methods*, 2011, **8**, 239–241.
22 S. Yao and O. Bakajin, *Anal. Chem.*, 2007, **79**, 5753–5759.
23 D. E. Hertzog, B. Ivorra, B. Mohammadi, O. Bakajin and J. G. Santiago, *Anal. Chem.*, 2006, **78**, 4299–4306.
24 Y. Li, Y. Xu, X. Feng and B. F. Liu, *Anal. Chem.*, 2012, **84**, 9025–9032.
25 O. Bilsel, C. Kayatekin, L. A. Wallace and C. R. Matthews, *Rev. Sci. Instrum.*, 2005, **76**, 0143021–0143027.
26 S. Matsumoto, A. Yane, S. Nakashima, M. Hashida, M. Fujita, Y. Goto and S. Takahashi, *J. Am. Chem. Soc.*, 2007, **129**, 3840–3841.
27 T. Egawa, J. L. Durand, E. Y. Hayden, D. L. Rousseau and S. R. Yeh, *Anal. Chem.*, 2009, **81**, 1622–1627.
28 Y. Li, D. Zhang, X. Feng, Y. Xu and B. F. Liu, *Talanta*, 2012, **88**, 175–180.
29 J. B. Knight, A. Vishwanath, J. P. Brody and R. H. Austin, *Phys. Rev. Lett.*, 1998, **80**, 3863–3866.
30 P. Chen, X. Feng, J. Sun, Y. Wang, W. Du and B. F. Liu, *Lab Chip*, 2010, **10**, 1472–1475.
31 D. C. Duffy, J. C. McDonald, O. J. Schueller and G. M. Whitesides, *Anal. Chem.*, 1998, **70**, 4974–4984.
32 W. K. Ridgeway, E. Seitaridou, R. Phillips and J. R. Williamson, *Nucleic Acids Res.*, 2009, **37**, e142.
33 L. Ying, J. J. Green, H. Li, D. Klenerman and S. Balasubramanian, *Proc. Natl. Acad. Sci. U. S. A.*, 2003, **100**, 14629–14634.
34 Y. C. Lin, Y. C. Chung and C. Y. Wu, *Biomed. Microdevices*, 2007, **9**, 215–221.
35 B. F. Liu, M. Ozaki, Y. Utsumi, T. Hattori and S. Terabet, *Anal. Chem.*, 2003, **75**, 36–41.
36 K. Hatakeyama, T. Tanaka, M. Sawaguchi, A. Iwadate, Y. Mizutani, K. Sasaki, N. Tateishi and T. Matsunaga, *Lab Chip*, 2009, **9**, 1052–1058.
37 Z. Wang, S. Y. Chin, C. D. Chin, J. Sarik, M. Harper, J. Justman and S. K. Sia, *Anal. Chem.*, 2009, **82**, 36–40.
38 C. C. Chang, I. C. Kuo, I. F. Ling, C. T. Chen, H. C. Chen, P. J. Lou, J. J. Lin and T. C. Chang, *Anal. Chem.*, 2004, **76**, 4490–4494.
39 N. Jing, Y. Li, W. Xiong, W. Sha, L. Jing and D. J. Tweardy, *Cancer Res.*, 2004, **64**, 6603–6609.
40 D. Sen and W. Gilbert, *Nature*, 1988, **334**, 364–366.
41 D. Sen and W. Gilbert, *Nature*, 1990, **344**, 410–414.
42 G. V. Tolstonog, G. Li, R. L. Shoeman and P. Traub, *DNA Cell Biol.*, 2005, **24**, 85–110.
43 X. Y. Zhuang, J. Tang, Y. H. Hao and Z. Tan, *J. Mol. Recognit.*, 2007, **20**, 386–391.
44 J. J. Green, L. Ying, D. Klenerman and S. Balasubramanian, *J. Am. Chem. Soc.*, 2003, **125**, 3763–3767.
45 J. L. Mergny, J. Gros, A. De Cian, A. Bourdoncle, F. Rosu, B. Saccà, L. Guittat, S. Amrane, M. Mills, P. Alberti *et al.*, in *Quadruplex Nucleic Acids*, ed. S. Neidle and S. Balasubramanian, The Royal Society of Chemistry, 2006, pp. 31–80.
46 E. E. Merkina and K. R. Fox, *Biophys. J.*, 2005, **89**, 365–373.

